



Alternative acid catalysts for the stable and selective direct conversion of CO₂/CO mixtures into light olefins

A. Portillo, A. Ateka^{*}, J. Ereña, J. Bilbao, A.T. Aguayo

Department of Chemical Engineering, University of the Basque Country, UPV/EHU, P.O. Box 644, 48080 Bilbao, Spain

ARTICLE INFO

Keywords:

CO₂
Syngas
Olefins
Tandem catalyst
Acid catalyst
Catalyst deactivation

ABSTRACT

Different acid catalysts (silicoaluminophosphates (SAPOs) -34, -18, and -11, and HZSM-5 zeolite) were tested as components of In₂O₃-ZrO₂/acid tandem catalysts in the direct synthesis of light olefins by hydrogenation of CO₂, CO and their mixture. The conversion and olefins yield and selectivity evidence that the presence of the large amount of strongly acidic sites in SAPO-34 favors the extent of the reaction mechanism with methanol as intermediate, minimizing secondary methanation reactions. In addition, the shape selectivity of SAPO-34 boosts olefins selectivity (mainly of propylene), limiting the extent of the secondary reactions for the formation of other hydrocarbons. Using SAPOs as acid catalysts enhances olefins selectivity when co-feeding CO₂ with CO. Despite all tandem catalysts undergo deactivation by coke deposition (mostly in the acid catalyst), a pseudo-steady state of stable remaining activity is acquired. From the study of the coke nature, soft and hard coke were discerned. For the complete regeneration of the SAPO-34 in the tandem catalyst, the stripping of the soft coke is not sufficient and the combustion at 500 °C of the hard coke (little developed) deposited on the micropores is required.

1. Introduction

Fulfilling the objectives of decarbonization and limiting temperature increase below 2 °C by the end of this century, boosts the research on strategies for CO₂ separation/capture [1–3] and valorization technologies [4,5]. In this scenario, the interest in the direct synthesis of olefins from CO₂ [6,7] relies on the fact that two priority objectives, of environmental and energy interest, are jointly addressed: helping to mitigate the emissions of greenhouse gases (GHG) and meeting the growing demand for olefins.

Light olefins are building blocks of the petrochemical industry, being ethylene and propylene the chemicals of highest demand and the market is expected to grow 5.85% annually until 2027 [7]. Currently, light olefins are mainly produced from oil-derived streams by steam cracking [8] and fluidized catalytic cracking (FCC) [9]. Nonetheless, the future of both processes is conditioned by their great energy consumption and high CO₂ emissions [10]. Likewise, in the MTO (methanol to olefins)

[11,12] and MTP (methanol to propylene) [13] processes, currently with coal and natural gas as raw materials, high CO₂ emissions are generated in the catalyst regeneration unit. Other alternatives for light olefins production with promising results, as paraffins dehydrogenation (PDH) [14], olefin metathesis (OM) [15] or oxidative coupling of methane (OCM) [16] are still in development stage.

The direct production of hydrocarbons through CO₂ hydrogenation reduces the immobilized assets and operation cost compared to the two-stage process. Moreover, the main advantage is that the extent of the hydrocarbon formation reaction shifts the thermodynamic limitation of CO₂ hydrogenation. The drawback is that the suitable reaction conditions for the integrated process are different (intermediate) from the optimal ones for each of the two reaction stages. Thus, designing a tandem catalyst combining suitable activity, selectivity and stability properties for the integrated process is a priority objective [17]. The process can be carried out through two routes; i) the modified Fischer-Tropsch (MFT) synthesis, combining a catalyst for the Fischer-Tropsch

Abbreviations: BET, Brunauer-Emmett-Teller; BJH, Barrett-Joyner-Halenda; CHA, Chabacite; COx, CO + CO₂; DME, Dimethyl ether; FCC, Fluid catalytic cracking; FT, Fischer-Tropsch; GC/MS, Gas chromatography/mass spectrometry; GHG, Greenhouse gas; ICDD, International centre for diffraction data; IZ, In₂O₃-ZrO₂; MFT, Modified Fischer-Tropsch; MS-5, Molecular sieve; MTO, Methanol to olefins; MTP, Methanol to propylene; OCM, Oxidative coupling of methane; OM, Olefin metathesis; OX, Metallic oxide; PDH, Paraffins dehydrogenation; PPQ, Porapak Q; rWGS, Reverse water gas shift; SAPO, Silicoaluminophosphate; SEM, Scanning electron microscopy; TOS, Time on stream; TPD, Temperature programmed desorption; TPO, Temperature programmed oxidation; XRD, X-Ray diffraction; ZEO, Zeotype.

^{*} Corresponding author.

E-mail address: ainara.ateka@ehu.es (A. Ateka).

<https://doi.org/10.1016/j.fuproc.2022.107513>

Received 27 July 2022; Received in revised form 14 September 2022; Accepted 18 September 2022

Available online 28 September 2022

0378-3820/© 2022 The Authors. Published by Elsevier B.V. This is an open access article under the CC BY-NC-ND license (<http://creativecommons.org/licenses/by-nc-nd/4.0/>).

(FT) synthesis (generally based on Fe or Co) and a zeotype [18]; ii) with oxygenates (methanol and DME) as intermediates, using an OX/ZEO tandem catalyst, prepared combining a metallic oxide (OX) as catalyst for oxygenates synthesis and an acid zeotype (ZEO) to selectively catalyze the conversion of these into hydrocarbons [19]. In both routes, the shape selectivity and acidity of the zeotype can be oriented towards the production of light olefins, aromatics or isoparaffinic gasoline, being better the prospects for the route with oxygenates as intermediates [20].

Among the metallic oxides used as oxygenates synthesis catalysts in tandem catalysts, In_2O_3 has shown high activity and selectivity to light olefins [21,22]. In the activity of In_2O_3 , the adsorption capacity of CO_2 in the surface $\text{In}_2\text{O}_{3-x}$ oxygen vacancies has a relevant role [23,24]. The use of a certain amount of ZrO_2 as promoter favors the creation of additional oxygen vacancies and increases the CO_2 adsorption capacity, contributing to increase conversion and selectivity to light olefins (decreasing the formation of CH_4 and CO) [25,26] when using In_2O_3 - ZrO_2 in a tandem catalyst. Spectroscopic studies verified that the presence of ZrO_2 also attenuates the formation and subsequent sintering of molten In^0 species increasing the stability of the catalyst [27–29].

The oxygenates synthesis mechanism in the direct hydrogenation of CO_2 into olefins on tandem catalysts takes place through two routes (whose relative importance depends on the catalyst) [30,31]: i) with CO as intermediate (formed through the reverse water gas shift (rWGS) reaction), and, ii) with the direct formation of formate species ($^*\text{HCOO}$) as intermediates. The formation of the C-C bonds of the light olefins proceeds through the well-established dual cycle mechanism from the methoxy intermediate species [32], with the preferential formation of propylene in the oligomerization/cracking cycle of olefins and of ethylene and propylene by dealkylation of arenes in the aromatics cycle [33–36]. The knowledge on the dual cycle mechanism for the MTO process, that is, the effects of the properties of the catalyst (shape selectivity, amount and nature of the acid sites) and the reaction conditions (temperature, space time, concentration of methanol) in the conversion, olefin selectivity and distribution, and catalyst stability (those based on SAPO-34 and HZSM-5 zeolite are the most studied) are well known [37–40]. However, the conditions and composition of the reaction medium are different in the direct synthesis of olefins from CO_2/CO and a metallic catalyst is present. These differences advise to conduct an in depth study of the performance of the acid catalysts under these conditions [41].

Consequently, to fill the gaps concerning the role of the acid catalyst properties, in this manuscript the performance of tandem catalysts with different shape selectivity and acidity has been compared: silicoaluminophosphates (SAPOs), SAPO-34, SAPO-18 and SAPO-11 and HZSM-5 zeolite. These acid catalysts have been tested in tandem with In_2O_3 - ZrO_2 metallic oxide catalyst under the reaction conditions required for the direct conversion of CO_2 and syngas mixtures into hydrocarbons, seeking for olefins production principally. The objective is to assess the effect of acidity and shape selectivity on the activity and selectivity. In addition, special attention has been paid to stability, which determines the viability of the process, by analyzing the deactivated catalysts and coke precursors retained in the porous structure. The catalytic tests were carried out feeding CO_2/CO mixtures. This co-feeding has received little attention in the literature [42], and is interesting from the perspective of sustainable production and circular economy, considering the possibility of co-feeding syngas derived from the gasification of biomass or waste from the consumer society (such as plastics, tires or sewage sludge).

2. Experimental

2.1. Catalyst description

The In_2O_3 - ZrO_2 (IZ) catalyst was synthesized following a co-precipitation method (at 70 °C and pH ~ 7) described in detail elsewhere [43] and with a Zr/In ratio of 1/2, which has been established to

maximize the synergy of the CO_2 adsorption and H_2 splitting capacities of ZrO_2 and In_2O_3 , respectively [44]. These catalysts were powdered, pelletized, crushed and sieved to 125–250 μm particle size range. The acid catalysts used have different acidity and shape selectivity and were selected pursuing olefins selectivity and stability. These catalysts were: Commercial SAPO-34 (ACS Materials) and HZSM-5 (Zeolyst International with a Si/Al ratio of 140); and SAPOs –18 and –11 prepared in the laboratory using a procedure based on the patent of the Union Carbide Corporation [45]. The HZSM-5 catalyst was provided by Zeolyst Int. in ammonium form and was calcined at 575 °C, for 2 h to obtain the acid form. SAPO-34 catalyst was calcined at 550 °C for 5 h. These acid catalysts were powdered, pelletized, crushed and sieved to 300–400 μm particle size range. The different particle size respect to IZ catalyst allowed analyzing the spent catalysts independently.

The tandem catalysts consist of a physical mixture of IZ and acid catalysts in a 2/1 mass ratio, which is considered suitable to favor the synergy of the stages of methanol/DME synthesis and selective conversion into olefins, minimizing their further conversion into paraffins [21].

2.2. Morphology and general properties of the acid catalysts

The selection of the acid catalysts was carried out based on shape selectivity and acidity, bearing in mind the well established effect of these properties on the performance for oxygenates conversion into olefins. The severe shape selectivity of SAPO-34, as a consequence of its structure (chabacite, CHA), with eight-membered ring pore openings $0.38 \times 0.38 \text{ nm}$, is adequate to avoid the extent of light olefins side reactions of cyclization, condensation-alkylation, hydrogen transfer and isomerization. In addition, the high H_2 pressure at the conditions for the direct synthesis of olefins contributes to minimizing coke formation in the $0.67 \times 0.94 \text{ nm}$ cavities of the SAPO-34 [46]. SAPO-18 (AEI framework) is isomorphic to SAPO-34, but with different orientation of the double-six rings and wider cavities (more elongated and with a broader base than those of the CHA structure) [47]. As a consequence of the differences in the cavities and their effect on the dual cycle mechanism, the resulting olefins selectivity in the MTO process is different. Ethylene and propylene are mainly formed with SAPO-34, whereas propylene and butylene with SAPO-18 [48]. Aguayo et al. [49] attribute to these differences in the porous structure the lower deactivation by coke of SAPO-18 than of SAPO-34 in the MTO process. SAPO-11, with an AEL framework consisting of 10-membered elliptical rings with $0.40 \times 0.65 \text{ nm}$ pores in one-dimensional arrays, has moderate acidity, low density of strong Brønsted sites and is highly stable in the MTO process [50].

HZSM-5 zeolite (MFI framework), with straight elliptical ($0.52 \times 0.56 \text{ nm}$) and zig-zag ($0.51 \times 0.55 \text{ nm}$) pores and without cages at the intersections, might be a good candidate as acid component of the tandem catalysts due to the versatility of its acidity. Hence, with moderate acidity and low density of strongly acid Brønsted sites, it is used for the selective production of propylene in the MTP process [13] and of ethylene and propylene from DME [51]. Stability is another key property of HZSM-5, and is optimized with a balance between the crystal size control and acidity regulation [52].

2.3. Catalyst characterization

As textural properties of the catalysts, the Brunauer–Emmett–Teller (BET) specific surface area (S_{BET}), micro- and total- pore volume, and average pore diameter were determined by N_2 Temperature Programmed Adsorption-Desorption analyses in a Micromeritics ASAP 2010 equipment. The procedure consisted on outgassing the sample at 150 °C under vacuum (10^{-3} mmHg) for 8 h to eliminate impurities and H_2O adsorbed on the surface, facilitating N_2 adsorption. Next, serial equilibrium stages of N_2 adsorption-desorption until the complete saturation of the sample at cryogenic liquid N_2 temperature (-196 °C) were carried out. Pore volume was calculated with the Barrett-Joyner-

Halenda (BJH) method using the adsorption branch of the isotherm.

The morphology of the catalysts was studied by Scanning Electron Microscopy (SEM) using a JEOL JSM-700F instrument equipped with a W filament. The images are gathered in Fig. S1 in the Supplementary Material. The structural properties were determined by X-Ray Diffraction (XRD) on a Bruker D8 Advance diffractometer equipped with a Ge primary monochromator, with Bragg-Brentano geometry and a Cu-K α radiation, wavelength of 1.5406Å.

The acidity was determined by Temperature Programmed Desorption of NH₃ (TPD-NH₃) in a Micromeritics Autochem 2920 equipment. The sample was first submitted to a pretreatment at 550 °C for 30 min with He (160 cm³ min⁻¹) for sweeping H₂O and impurities possibly absorbed. After the stabilization at 150 °C with He (20 cm³ min⁻¹), NH₃ injections (50 cm³ min⁻¹) were carried out at 150 °C for the complete saturation of the sample. Finally, after a sweeping with He (20 cm³ min⁻¹) for removing the adsorbate physically adsorbed, NH₃ desorption was conducted by heating the sample (5 °C min⁻¹ temperature rate) up to 550 °C.

The coke in the spent catalysts was characterized by Temperature Programmed Desorption in He atmosphere (HeTPD-GC/MS analysis) of the retained compounds (soft coke) and Temperature Programmed Oxidation (TPO) of the remaining coke (hard coke). For assuring reproducible results of coke characterization, previously the catalytic bed was subjected after each reaction to a sweeping in situ with N₂ (60 cm³ min⁻¹) for 30 min at reaction temperature in order to remove the adsorbed volatile products. Subsequently, the catalytic bed was cooled to room temperature and the catalysts (metallic and acid) were separated from the inert SiC for characterization. The HeTPD-GC/MS experiments were conducted at 500 °C in a CDS Pyroprobe® Model 6150 and the generated volatiles were transferred through a thermostatic line to a Shimadzu QP2010 GC/MS device provided with a BPX5 column (50 m × 0.22 mm × 0.25 µm film thickness) and MS detector (semi-quantitative composition based on % peak area). For the analysis in the GC/MS, a 7 °C min⁻¹ heating rate from 50 °C to 300 °C was used, and the identification of the compounds was carried out using NIST library. The TPO-GC/MS measurements were conducted in a TGA Q5000 IR thermobalance (TA Instruments) at a heating rate of 7 °C min⁻¹ up to 700 °C in air atmosphere (20 cm³ min⁻¹).

2.4. Reaction equipment, conditions and indices

The reaction runs were performed in a PID Eng&Tech Microactivity Reference equipment provided with an isothermal fixed bed reactor, described in detail elsewhere [43]. The reactor is made of 316 stainless steel, 9 mm internal diameter and 100 mm effective length. It can operate up to 700 °C, 100 bar and with up to 5 g catalyst loadings. The catalytic bed is composed of a mixture of catalyst and an inert solid (SiC) as to ensure isothermal conditions, without hot spots, and avoid preferential pathways. The product stream was heated up to 110 °C to avoid condensation problems, and analyzed online in a microGC Varian CP4900 gas-chromatograph. For this analysis three columns were used: i) Molecular sieve (MS-5) to quantify H₂, N₂, O₂ and CO; ii) Porapak Q (PPQ) for CO₂, water, C₁-C₄ hydrocarbons and methanol/DME; iii) 5CB column (CPSiL) for higher hydrocarbons. Typically, the reaction runs were carried out at 400 °C, 30 bar and H₂/CO_x ratio of 3, since these conditions were established as suitable for the joint valorization of CO₂ and syngas into olefins in the literature [26,43]. Typically, space time of 5 g_{tandem.cat} h mol⁻¹ was used, corresponding to 122 mg of In₂O₃-ZrO₂, 61 mg of acid catalyst, 45 cm³ min⁻¹ of H₂ and 15 cm³ min⁻¹ of CO₂/CO. CO₂/CO_x ratios in the feed of 0 (corresponding to syngas, H₂ + CO), 0.5 (H₂ + CO₂/CO, with 50% of CO + 50% of CO₂), and 1 (H₂ + CO₂) were used, to study the influence of the feed composition on the catalytic activity.

As reaction indices, conversion of CO₂ (X_{CO_2}) and CO_x (CO₂ + CO) (X_{CO_x}) were defined as:

$$\text{Conversion of CO}_2 : \quad (1)$$

$$X_{CO_2} = \frac{F_{CO_2}^0 - F_{CO_2}}{F_{CO_2}^0} \cdot 100$$

$$\text{Conversion of CO and CO}_2 : \quad (2)$$

$$X_{CO_x} = \frac{F_{CO_x}^0 - F_{CO_x}}{F_{CO_x}^0} \cdot 100$$

where $F_{CO_2}^0$ and F_{CO_2} are the molar flowrates of CO₂ in content C atoms, in the feed and product streams, respectively. Likewise, $F_{CO_x}^0$ and F_{CO_x} are those considering CO_x molar flowrates.

Products yields and selectivities (excluding CO and CO₂) were defined, by grouping the products into the following lumps: methane, C₂-C₄ olefins, C₂-C₄ paraffins and oxygenates (methanol and DME) according to the following expressions:

$$Y_i = \frac{n_i \cdot F_i}{F_{CO_x}^0} \cdot 100 \quad (3)$$

$$S_i = \frac{n_i \cdot F_i}{\sum_i (n_i \cdot F_i)} \cdot 100 \quad (4)$$

where n_i is the number of C atoms in a molecule of compound i and F_i the molar flowrate of the component in the product stream.

It should be noted that all the results presented are average values of at least 3 experiments carried out under the same operating conditions. The error with respect to the average is lower than 2% in all cases.

3. Results and discussion

In this section, first, the properties of the catalysts are disclosed, and subsequently, the influence of the acidity and shape selectivity of the acid catalysts on the performance (activity, selectivity and stability) of the IZ/acid tandem catalysts assessed for the direct conversion of CO₂ (and CO₂ + CO mixtures) into light olefins is analyzed. Finally, an insight into coke deactivation is provided.

3.1. Properties of the fresh catalysts

The physical properties (Table 1) derived from N₂ adsorption-desorption analyses evidenced that the three SAPOs have similar pore volume (V_p) (slightly higher for SAPO-34, 0.230 cm³ g⁻¹), but significant differences on BET specific surface area (S_{BET}). S_{BET} is outstandingly higher for SAPO-34 (652 m² g⁻¹) as a consequence of its micropore density (micro pore volume, V_{micro} , of 0.219 cm³ g⁻¹). The average pore diameter (d_p) is also different for the SAPOs, being the minimum value that for SAPO-34 (1.5 nm). SAPO-11 is the one with the lowest micropore density among the three SAPOs (due to its unidirectional arrangement), with V_{micro} of 0.043 cm³ g⁻¹, low S_{BET} of 124 m² g⁻¹ and d_p value of 3.3 nm. The properties of the HZSM-5 zeolite (S_{BET} = 376 m² g⁻¹, V_{micro} = 0.083 cm³ g⁻¹, V_p = 0.204 cm³ g⁻¹, d_p = 2.2 nm) can be considered relatively close to those of SAPO-18 (although somewhat lower V_{micro}). It can be seen that the structure of In₂O₃-ZrO₂ is exclusively mesoporous, with relatively low S_{BET} (86 m² g⁻¹) and d_p of 9 nm.

For analyzing the morphology of the catalysts, XRD patterns for the different catalysts are gathered in Fig. 1. As observed in the spectra, the

Table 1
Physical properties of the catalysts.

Catalyst	S_{BET} (m ² g ⁻¹)	V_{micro} (cm ³ g ⁻¹)	V_p (cm ³ g ⁻¹)	d_p (nm)
HZSM-5	376	0.083	0.204	2.2
SAPO-34	652	0.219	0.230	1.5
SAPO-18	381	0.141	0.202	2.1
SAPO-11	124	0.043	0.200	3.3
In ₂ O ₃ -ZrO ₂	86	-	0.23	9.0

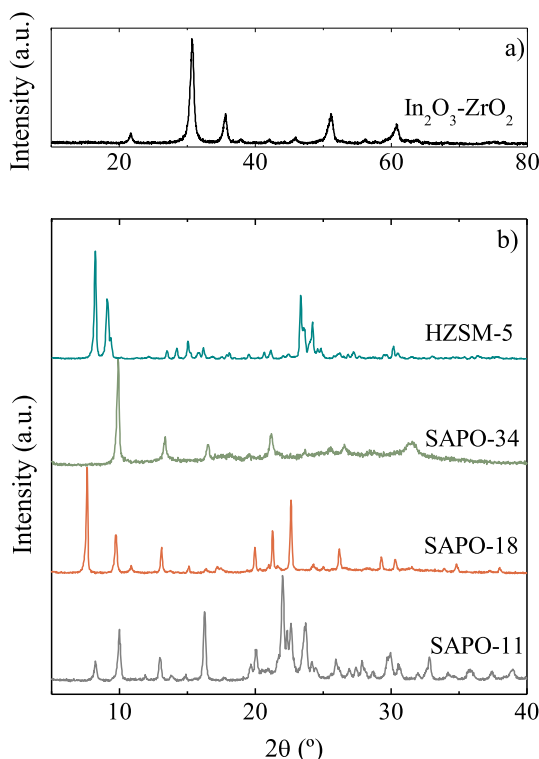


Fig. 1. XRD patterns for the $\text{In}_2\text{O}_3\text{-ZrO}_2$ metallic catalyst (a) and acid HZSM-5, S-34, S-18 and S-11 catalysts (b).

metallic $\text{In}_2\text{O}_3\text{-ZrO}_2$ catalyst is a combination of the peaks representative of pure In_2O_3 and ZrO_2 , at $2\theta = 21.68^\circ, 30.74^\circ, 35.61^\circ, 37.88^\circ, 40^\circ, 42.03^\circ, 43.99^\circ, 45.86^\circ, 51.14^\circ, 52.84^\circ, 56.14^\circ, 59.25^\circ, 60.78^\circ, 62.33^\circ, 63.79^\circ, 65.23, 68.16^\circ$ and 69.61° for In_2O_3 , in accordance with standard #71–2195 of ICDD (International Centre for Diffraction Data) and; at $2\theta = 30.68^\circ, 35.53^\circ, 51.03^\circ, 60.64^\circ, 63.09^\circ$ and 74.94° for ZrO_2 in accordance with standard ICDD #491642. The diffractograms of the acid catalysts are also characteristic of those materials [45].

The total acidity value and the acid strength distribution were determined from the $\text{NH}_3\text{-TPD}$ profiles in Fig. 2, distinguishing the relative amount of desorbed NH_3 in three temperature ranges (Table 2). According to the usual assignment in the literature [53], these ranges

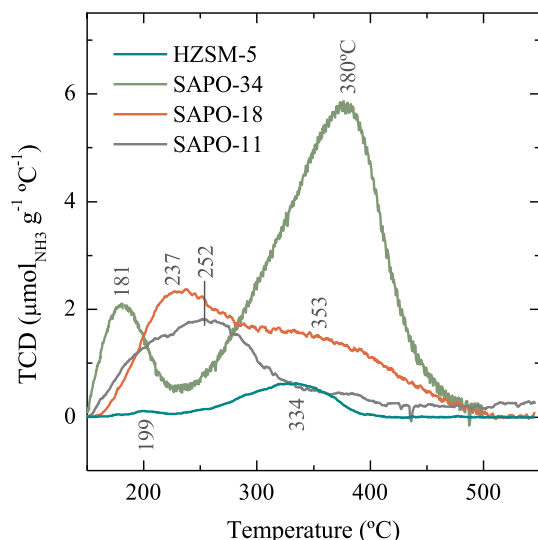


Fig. 2. $\text{NH}_3\text{-TPD}$ profiles for the acid HZSM-5, S-34, S-18 and S-11 catalysts.

Table 2
Acid properties of the catalysts.

Catalyst	Total Acidity ($\mu\text{mol}_{\text{NH}_3} \text{g}^{-1}$)	Weak acidity ($\mu\text{mol}_{\text{NH}_3} \text{g}^{-1}$)	Medium acidity ($\mu\text{mol}_{\text{NH}_3} \text{g}^{-1}$)	Strong acidity ($\mu\text{mol}_{\text{NH}_3} \text{g}^{-1}$)
HZSM-5	74	5	46	23
SAPO-34	778	99	160	519
SAPO-18	427	132	167	128
SAPO-11	281	132	132	17

correspond to weak (150–250 °C), moderate (250–350 °C) and strong (350–450 °C) acid sites. The order of the total acidity of the SAPOs is: SAPO-34 ($777 \mu\text{mol}_{\text{NH}_3} \text{g}^{-1}$) > SAPO-18 (427) > SAPO-11 (281). As to the acid strength distribution regards, SAPO-34 has the highest amount of strongest acid sites, $519 \mu\text{mol}_{\text{NH}_3} \text{g}^{-1}$. SAPO-18 has lower amount of these strong sites, and their main $\text{NH}_3\text{-TPD}$ peak is 27°C lower. In SAPO-11 the acid sites are of weak and moderate strength, and in HZSM-5 zeolite the acid sites are mainly of moderate strength.

3.2. Performance of the catalysts

The performance of the IZ/acid tandem catalysts is compared with that of the $\text{In}_2\text{O}_3\text{-ZrO}_2$ (IZ) catalyst in Fig. 3 in terms of conversion (X_{CO_2} and X_{CO_x}) and selectivity for equimolecular CO_2 and CO feed (CO_2/CO_x of 0.5) in the reaction conditions described in Section 2.3. These results correspond to values at 16 h on stream, time for which the catalyst reached a pseudo-steady state (Section 3.3). It is noteworthy that X_{CO_2} is similar for all the alternatives (with a value surpassing 20%), although there are remarkable differences in products distribution.

SAPO-34 and – 18 catalysts showed the most similar performance, with hydrocarbon (paraffins + olefins) selectivity exceeding 90% (over 95% with SAPO-18). However, hydrocarbon distribution differed: paraffins represented 25% and olefins 75% with SAPO-34, whereas 17% and 83%, respectively, with SAPO-18, with the downside of higher methane selectivity (8.8% vs 2.6% with SAPO-34). With these two SAPOs, the synergy of the two reaction stages is effective. CO_x conversion boosted from <1% attained with the IZ catalyst individually, to a remarkable X_{CO_x} value of 4.3% achieved with IZ/SAPO-34. The good behavior of SAPO-34 can be explained by its high acidity. The mainly strong nature of the acid sites (Table 2), is adequate for the generation of a high amount of methoxy ions for the activation of the methanol/DME formation mechanism from these intermediates and the subsequent development of the dual cycle mechanism. In addition, by favoring the formation of methoxy ions with the IZ/SAPO-34 tandem catalyst the

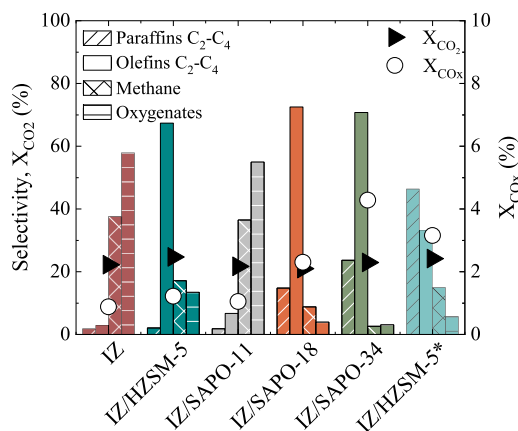


Fig. 3. Comparison of selectivity and conversion values obtained with the $\text{In}_2\text{O}_3\text{-ZrO}_2$ (IZ) catalyst and the IZ/acid tandem catalysts. Reaction conditions: CO_2/CO_x in the feed, 0.5; space time, $5 \text{ g}_{\text{tandem.catal}} \text{ h mol}^{-1}$ (122 mg $\text{In}_2\text{O}_3\text{-ZrO}_2$ and 61 mg acid catalyst, except for IZ-HZSM-5* catalyst, loading 643.55 mg of HZSM-5); time on stream, 16 h.

reverse WGS reaction is disfavored, suppressing CO by-product formation [54]. Whereas the density and strength of the acid sites of SAPO-18 is not sufficient for the formation of the amount of methoxy ions required to disfavor the CO₂ and CO methanation mechanisms occurring over the In₂O₃-ZrO₂ catalyst [43]. The absence of aromatics and the low paraffins yield with both catalysts is a consequence of the short extent of the secondary reactions (cyclization, condensation) which, together with hydrogen transfer (olefins to paraffins) are favored by the presence of strongly acidic Brønsted sites [55].

The reduced acidity of the HZSM-5 zeolite explains the limited extent of methanol conversion into olefins obtained with the IZ/HZSM-5 catalyst. As a result, olefins selectivity was slightly lower than that obtained with SAPOs –34 and –18, and the selectivity of unconverted oxygenates was high. Moreover, the significant selectivity of methane (17%) ratified the fact that the acidity of the HZSM-5 zeolite is not sufficient for shifting the methanation mechanism, characteristic of the In₂O₃-ZrO₂ catalyst in the absence of acid catalyst [43]. The lack of activity for the stage of oxygenate conversion was even more noticeable for IZ/SAPO-11 catalyst. High oxygenates yield was attained, resulting from the synthesis in the IZ catalyst (and the consequent selectivity of methane was also high), but olefins and paraffins selectivity scarce. Indeed, this catalyst resulted barely active for the dehydration of methanol to DME, being the former the main compound in the oxygenates stream. The activity of HZSM-5 and SAPO-11 for the conversion of oxygenates was low, implying that with these catalysts there is no synergy with the oxygenate synthesis stage and X_{COx} was very small. Consequently, the use of SAPO-11 for tandem catalyst was discarded in the following studies.

As to ascertain whether the performance of the tandem catalyst is related to its acidity, an additional run was carried out augmenting HZSM-5 catalyst loading (10.55 times higher) in the IZ/HZSM-5*, pursuing to achieve an equivalent total acidity of that of SAPO-34 (Table 2). The results plotted in Fig. 3 evidence that the approach almost tripled CO_x conversion, however, yielded paraffins as main products. That is, increasing space time of HZSM-5 in the tandem catalyst, paraffins selectivity increased from 2.1 to 46.3%, whereas olefins selectivity diminished from 67.4 to 33.1%, at almost equal methane selectivity. Therefore, the results confirm that not only a notable amount of acid sites is required for the selective production of olefins from CO₂/CO, but also the different shape selectivity, and the large difference in the content of strongly acidic sites between the catalyst used is relevant (519 μmol_{NH3} g⁻¹ in SAPO-34 and 23 μmol_{NH3} g⁻¹ in the HZSM-5 zeolite) (Table 2). It can be understood that the presence of these strong acid sites in SAPO-34 is important to favor the formation of methoxy ions, minimizing the extent of the alternative reactions of CO and CO₂ methanation [55]. The severe shape selectivity of this catalyst will contribute to the selective formation of olefins through the dual cycle mechanism [49].

Fig. 4 gathers the results for the hydrogenation of CO (CO₂/CO_x ratio of 0) (Fig. 4a) and CO₂ (CO₂/CO_x ratio of 1) (Fig. 4b) of the different catalysts sorted from left to right according to increasing acidity. It is observed that for the tandem catalysts (except for IZ/HZSM-5) hydrocarbon (paraffins + olefins + methane) selectivity over 90% was achieved whatever the CO₂/CO composition in the feed. Comparing the results in Figs. 3 and 4, it is observed that the co-feeding of CO₂ favors the extent of the route for olefins formation over the route for methanation with the tandem catalysts with SAPOs as acid catalysts. Thus, the joint conversion of CO and CO₂ upturned the selectivity of olefins from 53% for CO feeds (Fig. 4a) to >70% for CO₂/CO_x of 0.5 (Fig. 3) and 1 (Fig. 4b), for tandem catalyst with SAPO-34; and from 70% to 72.5% for tandem catalyst with SAPO-18. The effect of co-feeding CO₂ was higher over the undesired methane selectivity, decreasing from 9.8% for CO feeds (Fig. 4a) to 2.6% for CO₂/CO_x feeds in a ratio of 0.5 (Fig. 3) for tandem catalyst with SAPO-34, and from 9% to 4.7% with IZ/SAPO-18, and even lower for CO₂ feeds with both SAPOs (Fig. 4b). Unlikely, for the IZ/HZSM-5 catalyst, methane selectivity boosted for high CO₂

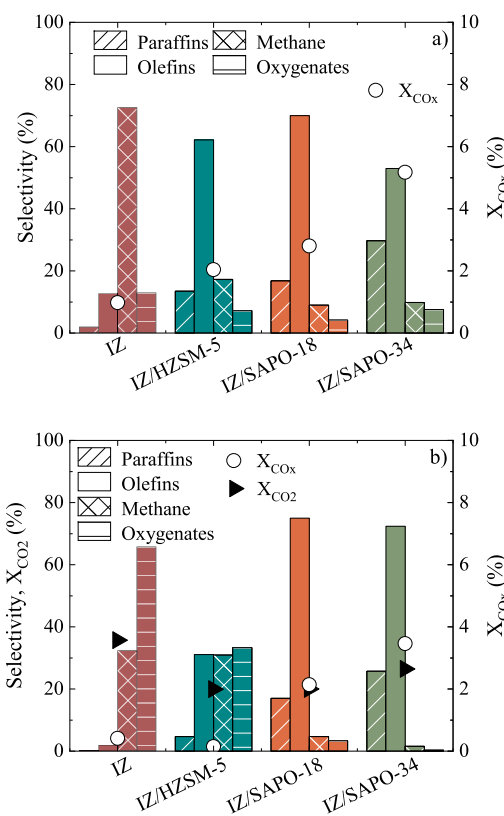


Fig. 4. Comparison of selectivity and conversion values obtained with the In₂O₃-ZrO₂ (IZ) catalyst and the IZ/acid tandem catalysts. a) CO₂/CO_x, 0. b) CO₂/CO_x, 1. Time on stream, 16 h.

contents in the feed, being the selectivity of methane as high as that of olefins (~31%) for CO₂ feeds (Fig. 4b), as a consequence of the acidity of this catalyst not being sufficient for shifting the methanation route.

In Fig. 5 the distribution (yields) of methane, C₂-C₄ paraffins and C₂-C₄ olefins for the different catalysts is compared. For CO feeds (CO₂/CO_x ratio of 0) (Fig. 5a) the highest yield of paraffins and olefins (Y_{O+P} of 4.17%) corresponds to the IZ/SAPO-34 catalyst. This yield was similar when CO₂ and CO were co-fed (Fig. 5b), with the advantage that methane yield decreased significantly (from 0.53 to 0.12%). Methane yield was even lower with CO₂ feeds (Fig. 5c), however, in this case the yield of olefins and paraffins (Y_{O+P} of 3.39%) was also lower.

For IZ/SAPO-18 catalyst and CO feeds, hydrocarbons yields were lower than those corresponding to IZ/SAPO-34 (Fig. 5a) and followed a different trend. The co-feeding of CO₂ slightly diminished C₂-C₄ hydrocarbons yields from those obtained with CO feeds (Fig. 5b) (Y_{O+P} from 2.02% to 1.9%), but upgraded that of methane over 50% (Y_{CH4} from 0.25% to 0.38%). For CO₂ feeds (Fig. 5c), hydrocarbons yield and also methane yield were lower than with other feeds, being the latter still higher than the methane yield corresponding to IZ/SAPO-34.

IZ/HZSM-5 catalyst gave way to the lowest C₂-C₄ olefins and paraffins yields, and this diminished upon increasing the CO₂ content in the feed, from Y_{O+P} of 1.5% for CO₂/CO_x ratio of 0 in the feed (Fig. 5b), to 0.05% for CO₂/CO_x of 1 (Fig. 5c).

For a clear visualization of the influence of the feed composition in the distribution of the target products, olefin yields obtained with the different catalysts are segregated in Fig. 6. The results evidence the highest yield of olefins was achieved with IZ/SAPO-34 catalyst and that propylene was the main product with the three catalysts and for all the feeds. For the catalyst with the two SAPOs, the effect of co-feeding CO and CO₂ on favoring the increase of ethylene and propylene yields is to be highlighted over the results achieved feeding CO and CO₂ individually. In addition, it is observed that the highest propylene/ethylene ratio

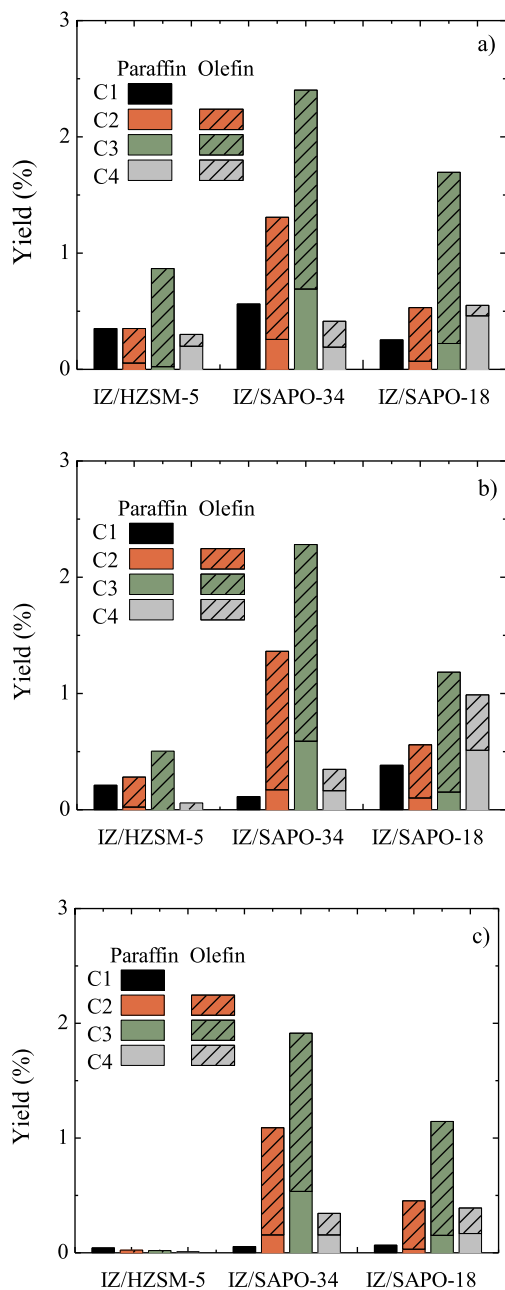


Fig. 5. Comparison of individual hydrocarbon yields obtained with the $\text{In}_2\text{O}_3\text{-ZrO}_2$ (IZ) catalyst and the IZ/acid tandem catalysts. a) CO_2/CO_x , 0, b) 0.5, and c) 1. Time on stream, 16 h.

was obtained with SAPO-18 regardless the feed composition (2.9 for CO feed and 2.1 for CO_2).

3.3. Deactivation of the catalysts and coke characteristics

In Fig. 7 the evolution of olefins yield with time on stream (TOS) is represented for the CO_2/CO_x ratio of 0.5 in the feed. Under these conditions, the catalysts undergo deactivation due to coke deposition as discussed later on (Table 3). Thus, for IZ/SAPO-34 catalyst, olefins yield decreased a 21%, from 3.6% to 3% after 16 h TOS. This lessening was relatively higher (48%) for IZ/HZSM-5 catalyst. As to IZ/SAPO-18 catalyst regards, an initial induction period is observed in the first ~2 h of reaction, presumably due to the time required by the dual cycle mechanism activation, being more significant with this catalyst. This

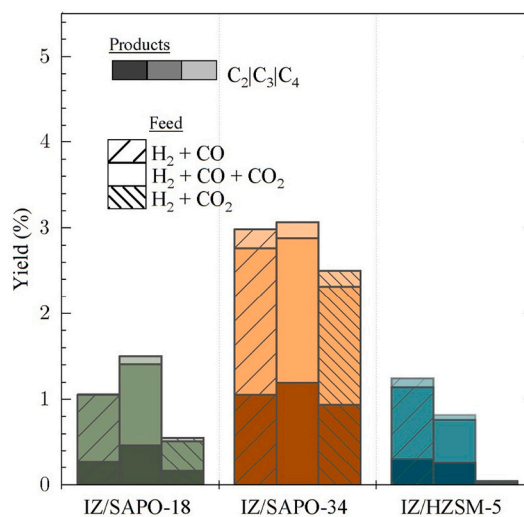


Fig. 6. Effect of the feed CO_2/CO composition on the yield of each olefin for the different tandem catalysts. Time on stream, 16 h.

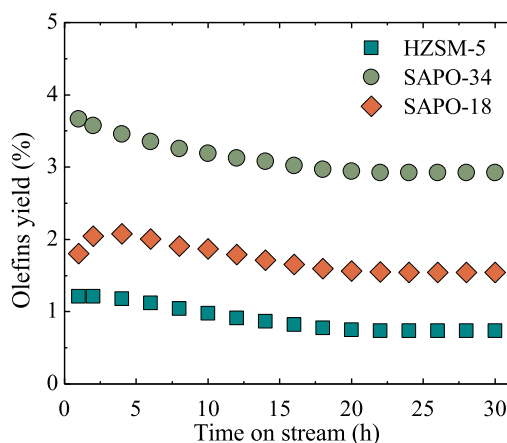











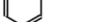






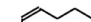







Fig. 7. Evolution of olefins yield with TOS for the different catalysts.

observation is consistent with the results with SAPO-18 in the conversion of methanol to olefins [56]. In Fig. 8 a faster lessening of paraffins yield than of olefins is observed. This feature indicates that activity decline due to coke deposition, results in a lower extent of the secondary reactions of olefins hydrogenation and hydrogen transfer.

In addition, it should be noted that the deactivation of the three catalysts is particularly slower than that obtained in the literature in the conversion of methanol/DME to hydrocarbons at atmospheric pressure with similar catalysts [11,12,57]. This difference is especially relevant for the SAPO-34 catalyst, which is completely deactivated in <1 h in the MTO process at 400 °C [58]. This lower deactivation in the direct synthesis of hydrocarbons is due to the hydrogenation of coke precursors at such high H_2 pressure.

Furthermore, according to the results in Figs. 7 and 8, it is relevant that after approximately 16 h TOS for the catalysts with SAPOs and 20 h for the catalyst with HZSM-5, a pseudo-steady state was reached, where deactivation was insignificant and the yields remained constant with TOS. The evolution of products yields with TOS and the existence of a pseudo-steady state is a consequence of the deactivating coke mechanism, which is disfavored by the presence of high H_2 pressure [59,60]. Additionally, it can be seen in Fig. 7 that the initial deactivation rate is in accordance with the acidity (Table 2): SAPO-34 > SAPO-18 > HZSM-5, which is explained because the mechanism of condensed coke structures formation is activated by the acid sites, specially by the strongly acid

Table 3
Main compounds detected in the soft coke by HeTPD-GC/MS analyses of the spent catalysts.

Catalyst	Molecule	Compound
IZ/SAPOs and IZ/HZSM-5		Hexene
		Hexadiene
		Hexadien-3-yne
		Heptene
		Toluene
		Octene
		Nonene
		Decene
		Undecene
		Dodecene
		Tridecene
		Tetradecene
		Hexadecene
		o-xylene
	IZ/HZSM-5	
		Nonanal
		Naphthalenes
		Oxigenated compounds
		Benzenes
		Benzenes
		Benzenes
		Benzenes
		Benzenes
		Benzenes

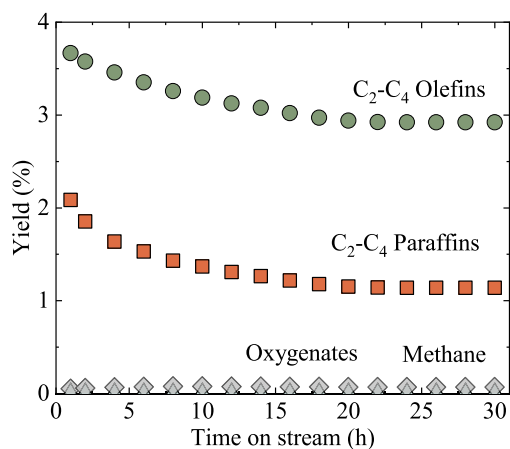


Fig. 8. Evolution of products distribution with TOS for IZ/SAPO-34 catalyst.

Brønsted sites [61,62]. The trend of the catalysts towards a pseudo-steady state of remarkable remaining activity is explained by the fact that a pseudo-equilibrium is reached between the stages of hydrogenation (activated by the IZ catalyst) and of dehydrogenation of coke precursors. The remaining activity of the catalyst in this state of pseudo-stability will depend on the properties of the catalyst and the composition of the reaction medium, in which, in addition to the H₂ pressure, also the concentration of H₂O attenuates the rate of coke formation [63–65].

The deactivation results in Figs. 7 and 8 are explained analyzing the coke deposited on the spent catalysts. In the coke two fractions can be distinguished. The fraction removable by stripping (soft coke) and the remaining fraction that requires combustion for its elimination (hard coke). The composition of the soft coke was determined by HeTPD-GC/MS measurements following the methodology described in section 2.2. In Fig. 9 the chromatograms of soft coke for the different catalysts are shown. In Table 3 the main compounds are listed. Linear olefin chains

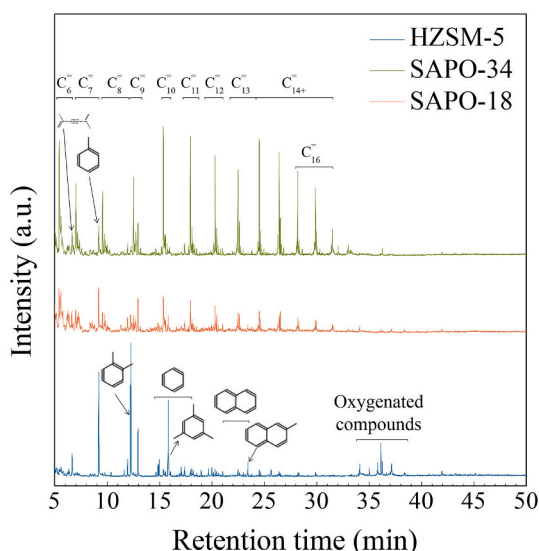


Fig. 9. Results of the HeTPD/GC-MS analysis of the soft coke of the spent acid catalysts. CO_2/CO_x , 0.5; time on stream, 16 h.

with 1, 2 or 3C=C bonds were observed for the catalyst with SAPO-34, with toluene as the only aromatic in a significant amount. In contrast, for the catalyst with HZSM-5, besides these compounds were detected, the presence of aromatics with 1 and 2 rings was way more relevant. Indeed, long linear chains of compounds with oxygenated C=O and C-OH groups also desorbed. The explanation for the unlike composition of the soft coke is the different capacity of the SAPOs and the HZSM-5 catalysts for the confinement of the soft coke. In the former, soft coke is confined in the cavities of the framework [64,66], and only the linear compounds with remarkable diffusivity are desorbed, leaving the aromatics retained. The diffusivity of these aromatics is greater in the HZSM-5 catalyst, due to the high degree of pore-crossings and the non-existence of cavities. Therefore, these aromatics, with methyl and ethyl groups, and even long oxygenated chains, were desorbed subsequently after the linear C_{16} chains.

The air TPO analyses of the spent catalyst (Section 2.3), after a TPD treatment in He stream, evidence the presence of a significant amount of retained coke (hard coke) that requires combustion for its removal. Furthermore, the separate TPO analyses of hard coke in the $\text{In}_2\text{O}_3\text{-ZrO}_2$ and in each acid catalyst of the tandem catalysts allowed verifying that the hard coke content in the acid catalysts was remarkably higher, being 0.66 wt% for the IZ and 4.67 wt% for the SAPO-34 in the spent IZ/SAPO-34 tandem catalyst. Table 4 gathers the hard coke contents measured from TPO analysis of the spent acid catalysts, and the temperature corresponding to the maximum combustion rate (position of the peak in the TPO profiles), indicative of the location and nature of coke.

The hard coke content follows the order: SAPO-34 > SAPO-18 > HZSM-5, in accordance with the order of acidity, thus, amount and strength of the acid sites (Table 2). This result is consistent with the well-established role of the acid sites in coke formation reactions from methanol/DME [62,67]. Furthermore, it is observed that combustion of the hard coke could be carried out at moderate temperature (even lower than 500 °C), considering that the maximum combustion peak in the TPO profile is obtained at 421 °C (Table 4), which is interesting because catalyst regeneration is facilitated, with no damage of the crystalline structure of the catalyst, and recovering its activity.

As observed in Table 4, the hard coke content in SAPO-18 is greater than expected from its acidity. This fact can be attributed to the ability of its porous structure (slightly different than that of SAPO-34 [47]) to retain soft coke molecules, which would condense to structures with low H/C ratio, explaining the high temperature related to the maximum rate of hard coke combustion (452 °C). The limited acidity of the HZSM-5

Table 4

Hard coke contents and combustion temperatures for the spent acid catalysts.

Catalyst	Hard coke content (%)	Main peak combustion temperature (°C)
HZSM-5	1.20	476
SAPO-34	4.67	421
SAPO-18	4.51	452

catalyst, with moderate amount of sites of weak acidic strength (Table 2), can explain the reduced hard coke content deposited (1.20 wt %) and the low deactivation rate (Fig. 8). Nevertheless, the high temperature required for the combustion of that coke (476 °C) is noteworthy. The explanation may be related to the low activity of this catalyst for the conversion of methanol/DME, which favors the formation of coke from intermediate methoxy ions. Additionally, due to the limited activity for cracking the side polymethylbenzene chains (intermediates in the dual cycle mechanism), these will condense to the polyaromatic chains of hard coke [68].

4. Conclusions

The performance (yield, selectivity and stability) of the $\text{In}_2\text{O}_3\text{-ZrO}_2/\text{acid}$ tandem catalysts in the synthesis of light olefins from CO and CO_2 is very sensitive to the properties of the acid catalyst. The good performance of the $\text{In}_2\text{O}_3\text{-ZrO}_2/\text{SAPO-34}$ catalyst may be attributed to the high density of strongly acid sites ($\text{NH}_3\text{-TPD}$ over 350 °C) of SAPO-34 and its severe shape selectivity.

These properties favor the formation of intermediate methoxy ions and their selective conversion into olefins via the dual cycle mechanism, favoring the synergy with methanol/DME synthesis and minimizing the extent of secondary reactions, such as methanation and paraffin formation. Yielding therefore, propylene as main product. In addition, with the $\text{In}_2\text{O}_3\text{-ZrO}_2/\text{SAPO-34}$ catalyst, olefins yield and selectivity increase with co-feeding CO and CO_2 , with respect to their individual valorization.

Coke deposition is the cause of deactivation of the tandem catalysts, which reach a pseudo-steady state of remarkable remaining activity. The study on the nature of coke (mainly present in the acid catalyst), distinguishing the fraction of soft coke and hard coke, reveals that the regeneration of the $\text{In}_2\text{O}_3\text{-ZrO}_2/\text{SAPO-34}$ catalyst requires the combustion of the hard coke with air. This can be performed at moderate temperature (500 °C) avoiding any damage of the catalyst.

CRediT authorship contribution statement

A. Portillo: Conceptualization, Methodology, Investigation, Validation, Data curation, Writing – original draft, Writing – review & editing. **A. Ateka:** Conceptualization, Methodology, Investigation, Validation, Data curation, Writing – original draft, Writing – review & editing. **J. Ereña:** Data curation, Writing – original draft. **J. Bilbao:** Conceptualization, Methodology, Investigation, Data curation, Writing – original draft, Writing – review & editing, Supervision. **A.T. Aguayo:** Project administration, Conceptualization, Supervision, Validation, Data curation.

Declaration of Competing Interest

The authors declare that they have no known competing financial interests or personal relationships that could have appeared to influence the work reported in this paper.

Data availability

The authors are unable or have chosen not to specify which data has been used.

Acknowledgements

This work has been carried out with the financial support of the Ministry of Science, Innovation and Universities of the Spanish Government (PID2019-108448RB-I00); the Basque Government (Project IT1645-22), the European Regional Development Funds (ERDF) and the European Commission (HORIZON H2020-MSCA RISE-2018. Contract No. 823745). A. Portillo is grateful for the Ph.D. grant from the Ministry of Science, Innovation and Universities of the Spanish Government (BES2017-081135). The authors thank for technical and human support provided by SGIker (UPV/EHU).

Appendix A. Supplementary data

Supplementary data to this article can be found online at <https://doi.org/10.1016/j.fuproc.2022.107513>.

References

- [1] H. Abdolahi-Mansoorkhani, S. Seddighi, CO₂ capture by modified hollow fiber membrane contactor: Numerical study on membrane structure and membrane wettability, *Fuel Process. Technol.* 209 (2020), 106530, <https://doi.org/10.1016/J.FUPROC.2020.106530>.
- [2] B. Aghel, S. Behaein, F. Alobiad, CO₂ capture from biogas by biomass-based adsorbents: A review, *Fuel*. 328 (2022), 125276, <https://doi.org/10.1016/J.FUEL.2022.125276>.
- [3] M. Sun, X. Zhu, C. Wu, O. Masek, C.H. Wang, J. Shang, Y.S. Ok, D.C.W. Tsang, Customizing high-performance molten salt biochar from wood waste for CO₂/N₂ separation, *Fuel Process. Technol.* 234 (2022), 107319, <https://doi.org/10.1016/J.FUPROC.2022.107319>.
- [4] A.D.N. Kamkeng, M. Wang, J. Hu, W. Du, F. Qian, Transformation technologies for CO₂ utilisation: current status, challenges and future prospects, *Chem. Eng. J.* 409 (2021), 128138, <https://doi.org/10.1016/j.cej.2020.128138>.
- [5] A. Ateka, P. Rodriguez-Vega, J. Ereña, A.T. Aguayo, J. Bilbao, A review on the valorization of CO₂. Focusing on the thermodynamics and catalyst design studies of the direct synthesis of dimethyl ether, *Fuel Process. Technol.* 233 (2022), 107310, <https://doi.org/10.1016/J.FUPROC.2022.107310>.
- [6] T. Numpilai, S. Kahadit, T. Wittoon, B.V. Ayodele, C.K. Cheng, N. Siri-Nguan, T. Sorchamni, C. Wattanakit, M. Chareonpanich, J. Limtrakul, CO₂ hydrogenation to light olefins over In₂O₃/SAPO-34 and Fe-CO/K-Al₂O₃ composite catalyst, *Top. Catal.* 1 (2021) 3, <https://doi.org/10.1007/s11244-021-01412-5>.
- [7] O.A. Ojelade, S.F. Zaman, A review on CO₂ hydrogenation to lower olefins: understanding the structure-property relationships in heterogeneous catalytic systems, *J. CO₂ Util.* 47 (2021), 101506, <https://doi.org/10.1016/J.JCOU.2021.101506>.
- [8] Z. Gholami, F. Gholami, Z. Tisler, M. Vakili, A review on the production of light olefins using steam cracking of hydrocarbons, *Energies* 14 (2021) 8190, <https://doi.org/10.3390/EN14048190>.
- [9] Z. Gholami, F. Gholami, Z. Tisler, M. Tomas, M. Vakili, A review on production of light olefins via fluid catalytic cracking, *Energies* 14 (2021) 1089, <https://doi.org/10.3390/EN14041089>.
- [10] F. Güleç, A. Erdogan, P.T. Clough, E. Lester, Investigation of the hydrodynamics in the regenerator of fluid catalytic cracking unit integrated by chemical looping combustion, *Fuel Process. Technol.* 223 (2021), 106998, <https://doi.org/10.1016/J.FUPROC.2021.106998>.
- [11] P. Tian, Y. Wei, M. Ye, Z. Liu, Methanol to olefins (MTO): from fundamentals to commercialization, *ACS Catal.* 5 (2015) 1922–1938, <https://doi.org/10.1021/acscatal.5b00007>.
- [12] T. Cordero-Lanzac, A.T. Aguayo, A.G. Gayubo, J. Bilbao, Consideration of the activity distribution using the population balance theory for designing a dual fluidized bed reactor-regenerator system. Application to the MTO process, *Chem. Eng. J.* 405 (2021), 126448, <https://doi.org/10.1016/J.CEJ.2020.126448>.
- [13] P. Zhang, L. Ma, F. Meng, L. Wang, R. Zhang, G. Yang, Z. Li, Boosting CO₂ hydrogenation performance for light olefin synthesis over GaZrOx combined with SAPO-34, *Appl. Catal. B Environ.* 305 (2022), 121042, <https://doi.org/10.1016/J.APCATB.2021.121042>.
- [14] A. Agrawal, O. Singh, B.M. Abraham, S.R. Yenumala, A. Ray, B. Sarkar, Low-temperature selective production of propylene from non-oxidative dehydrogenation of propane over unconventional Zr/ZK-5 catalysts, *Fuel Process. Technol.* 235 (2022), 107362, <https://doi.org/10.1016/J.FUPROC.2022.107362>.
- [15] X. Chen, J. Liu, H. Yan, X. Zhou, S. Yao, Y. Wang, W. Liang, Z. Guo, Y. Liu, X. Feng, X. Jin, C. Yang, Insight into the effect of Lewis Acid of W/Al-MCM-41 Catalyst on Metathesis of 1-Butene and Ethylene, *Appl. Catal. A Gen.* 604 (2020), 117772, <https://doi.org/10.1016/J.APCATA.2020.117772>.
- [16] A.M. Arinaga, M.C. Ziegelski, T.J. Marks, Alternative oxidants for the catalytic oxidative coupling of methane, *Angew. Chem. Int. Ed.* 60 (2021) 10502–10515, <https://doi.org/10.1002/ANIE.202012862>.
- [17] S. De, A. Dokania, A. Ramirez, J. Gascon, Advances in the design of heterogeneous catalysts and thermocatalytic processes for CO₂ utilization, *ACS Catal.* 10 (2020) 14147–14185, <https://doi.org/10.1021/acscatal.0c04273>.
- [18] B. Pawelec, R. Guil-López, N. Mota, J.L.G. Fierro, R.M. Navarro Yerga, Catalysts for the conversion of CO₂ to low molecular weight olefins—a review, *Materials (Basel)*. 14 (2021) 6952, <https://doi.org/10.3390/ma14226952>.
- [19] P. Sharma, J. Sebastian, S. Ghosh, D. Creaser, L. Olsson, Recent advances in hydrogenation of CO₂ into hydrocarbons via methanol intermediate over heterogeneous catalysts, *Catal. Sci. Technol.* 11 (2021) 1665–1697, <https://doi.org/10.1039/D0CY01913E>.
- [20] A. Ramirez, X. Gong, M. Caglayan, S.A.F. Nastase, E. Abou-Hamad, L. Gevers, L. Cavallo, A. Dutta Chowdhury, J. Gascon, Selectivity descriptors for the direct hydrogenation of CO₂ to hydrocarbons during zeolite-mediated bifunctional catalysis, *Nat. Commun.* 121 (12) (2021) 1–13, <https://doi.org/10.1038/s41467-021-26090-5>.
- [21] T. Numpilai, C. Wattanakit, M. Chareonpanich, J. Limtrakul, T. Wittoon, Optimization of synthesis condition for CO₂ hydrogenation to light olefins over In₂O₃ admixed with SAPO-34, *Energy Convers. Manag.* 180 (2019) 511–523, <https://doi.org/10.1016/J.ENCONMAN.2018.11.011>.
- [22] S. Wang, P. Wang, Z. Qin, W. Yan, M. Dong, J. Li, J. Wang, W. Fan, Enhancement of light olefin production in CO₂ hydrogenation over In₂O₃-based oxide and SAPO-34 composite, *J. Catal.* 391 (2020) 459–470, <https://doi.org/10.1016/J.JCAT.2020.09.010>.
- [23] S. Ghosh, J. Sebastian, L. Olsson, D. Creaser, Experimental and kinetic modeling studies of methanol synthesis from CO₂ hydrogenation using In₂O₃ catalyst, *Chem. Eng. J.* 416 (2021), 129120, <https://doi.org/10.1016/j.cej.2021.129120>.
- [24] J. Wang, G. Zhang, J. Zhu, X. Zhang, F. Ding, A. Zhang, X. Guo, C. Song, CO₂ hydrogenation to methanol over In₂O₃-based catalysts: from mechanism to catalyst development, *ACS Catal.* 11 (2021) 1406–1423, <https://doi.org/10.1021/acscatal.0c03665>.
- [25] S. Dang, P. Gao, Z. Liu, X. Chen, C. Yang, H. Wang, L. Zhong, S. Li, Y. Sun, Role of zirconium in direct CO₂ hydrogenation to lower olefins on oxide/zeolite bifunctional catalysts, *J. Catal.* 364 (2018) 382–393, <https://doi.org/10.1016/j.jcat.2018.06.010>.
- [26] P. Gao, S. Dang, S. Li, X. Bu, Z. Liu, M. Qiu, C. Yang, H. Wang, L. Zhong, Y. Han, Q. Liu, W. Wei, Y. Sun, Direct production of lower olefins from CO₂ conversion via bifunctional catalysis, *ACS Catal.* 8 (2018) 571–578, <https://doi.org/10.1021/acscatal.7b02649>.
- [27] T.P. Araújo, A. Shah, C. Mondelli, J.A. Stewart, D. Curulla Ferré, J. Pérez-Ramírez, Impact of hybrid CO₂-CO feeds on methanol synthesis over In₂O₃-based catalysts, *Appl. Catal. B Environ.* 285 (2021), 119878, <https://doi.org/10.1016/J.APCATB.2021.119878>.
- [28] A. Tsoukalou, P.M. Abdala, D. Stoian, X. Huang, M.G. Willinger, A. Fedorov, C. R. Müller, Structural evolution and dynamics of an In₂O₃ catalyst for CO₂ hydrogenation to methanol: an operando XAS-XRD and in situ TEM study, *J. Am. Chem. Soc.* 141 (2019) 13497–13505, <https://doi.org/10.1021/jacs.9b04873>.
- [29] S. Zhang, Z. Wu, X. Liu, K. Hua, Z. Shao, B. Wei, C. Huang, H. Wang, Y. Sun, A Short review of recent advances in direct CO₂ hydrogenation to alcohols, *Top. Catal.* 64 (2021) 371–394, <https://doi.org/10.1007/S11244-020-01405-W>.
- [30] X. Jiang, X. Nie, X. Guo, C. Song, J.G. Chen, Recent advances in carbon dioxide hydrogenation to methanol via heterogeneous catalysis, *Chem. Rev.* 120 (2020) 7984–8034, <https://doi.org/10.1021/acs.chemrev.9b00723>.
- [31] J. Zhong, X. Yang, Z. Wu, B. Liang, Y. Huang, T. Zhang, State of the art and perspectives in heterogeneous catalysis of CO₂ hydrogenation to methanol, *Chem. Soc. Rev.* 49 (2020) 1385–1413, <https://doi.org/10.1039/c9cs00614a>.
- [32] Y. Jiang, W. Wang, V.R.R. Marthala, J. Huang, B. Sulikowski, M. Hunger, Effect of organic impurities on the hydrocarbon formation via the decomposition of surface methoxy groups on acidic zeolite catalysts, *J. Catal.* 238 (2006) 21–27, <https://doi.org/10.1016/j.jcat.2005.11.029>.
- [33] M. Björger, S. Svelle, F. Joensen, J. Nerlov, S. Kolboe, F. Bonino, L. Palumbo, S. Bordiga, U. Olsbye, Conversion of methanol to hydrocarbons over zeolite H-ZSM-5: on the origin of the olefinic species, *J. Catal.* 249 (2007) 195–207, <https://doi.org/10.1016/j.jcat.2007.04.006>.
- [34] S. Ilias, A. Bhan, Mechanism of the catalytic conversion of methanol to hydrocarbons, *ACS Catal.* 3 (2013) 18–31, <https://doi.org/10.1021/cs3006583>.
- [35] W. Dai, C. Wang, M. Dymbala, G. Wu, N. Guan, L. Li, Z. Xie, M. Hunger, Understanding the early stages of the methanol-to-olefin conversion on H-SAPO-34, *ACS Catal.* 5 (2015) 317–326, <https://doi.org/10.1021/cs5015749>.
- [36] I. Yarulina, A.D. Chowdhury, F. Meirer, B.M. Weckhuysen, J. Gascon, Recent trends and fundamental insights in the methanol-to-hydrocarbons process, *Nat. Catal.* 16 (1) (2018) 398–411, <https://doi.org/10.1038/s41929-018-0078-5>.
- [37] D. Li, B. Xing, B. Wang, R. Li, Activity and selectivity of methanol-to-olefin conversion over Zr-modified H-SAPO-34/H-ZSM-5 zeolites - A theoretical study, *Fuel Process. Technol.* 199 (2020), 106302, <https://doi.org/10.1016/J.FUPROC.2019.106302>.
- [38] N. Hadi, A. Farzi, A review on reaction mechanisms and catalysts of methanol to olefins process, *Chem. Eng. Commun.* (2021) 1–47, <https://doi.org/10.1080/00986445.2021.1983547>.
- [39] Z. Shi, A. Bhan, Tuning the ethylene-to-propylene ratio in methanol-to-olefins catalysis on window-cage type zeolites, *J. Catal.* 395 (2021) 266–272, <https://doi.org/10.1016/J.JCAT.2021.01.015>.
- [40] Z. Yang, L. Zhang, Y. Zhou, H. Wang, L. Wen, E. Kianfar, Investigation of effective parameters on SAPO-34 nanocatalyst in the methanol-to-olefin conversion process: a review, *Rev. Inorg. Chem.* 40 (2020) 91–105, <https://doi.org/10.1515/REVIC-2020-0003/MACHINEREADEABLECITATION/RIS>.
- [41] J. Zhong, J. Han, Y. Wei, Z. Liu, Catalysts and shape selective catalysis in the methanol-to-olefin (MTO) reaction, *J. Catal.* 396 (2021) 23–31, <https://doi.org/10.1016/J.JCAT.2021.01.027>.

- [42] X. Liu, M. Wang, H. Yin, J. Hu, K. Cheng, J. Kang, Q. Zhang, Y. Wang, Tandem catalysis for hydrogenation of CO and CO₂ to lower olefins with bifunctional catalysts composed of spinel oxide and SAPO-34, *ACS Catal.* 10 (2020) 8303–8314, <https://doi.org/10.1021/acscatal.0c01579>.
- [43] A. Portillo, A. Ateka, J. Ereña, A.T. Aguayo, J. Bilbao, Conditions for the joint conversion of CO₂ and syngas in the direct synthesis of light olefins using In₂O₃-ZrO₂/SAPO-34 catalyst, *Ind. Eng. Chem. Res.* 61 (2021) 10365–10376, <https://doi.org/10.1021/ACS.IECR.1C03556>.
- [44] A. Portillo, A. Ateka, J. Ereña, J. Bilbao, A.T. Aguayo, Role of Zr loading into In₂O₃ catalysts for the direct conversion of CO₂/CO mixtures into light olefins, *J. Environ. Manag.* 316 (2022), 115329, <https://doi.org/10.1016/j.jenvman.2022.115329>.
- [45] M. Sánchez-Contador, A. Ateka, A.T. Aguayo, J. Bilbao, Behavior of SAPO-11 as acid function in the direct synthesis of dimethyl ether from syngas and CO₂, *J. Ind. Eng. Chem.* 63 (2018) 245–254, <https://doi.org/10.1016/j.jiec.2018.02.022>.
- [46] X. Zhao, J. Li, P. Tian, L. Wang, X. Li, S. Lin, X. Guo, Z. Liu, Achieving a Superlong lifetime in the zeolite-catalyzed MTO reaction under high pressure: synergistic effect of hydrogen and water, *ACS Catal.* 9 (2019) 3017–3025, <https://doi.org/10.1021/acscatal.8b04402>.
- [47] D.S. Wragg, D. Akporiaye, H. Fjellvåg, Direct observation of catalyst behaviour under real working conditions with X-ray diffraction: comparing SAPO-18 and SAPO-34 methanol to olefin catalysts, *J. Catal.* 279 (2011) 397–402, <https://doi.org/10.1016/j.jcat.2011.02.011>.
- [48] J. Zhong, J. Han, Y. Wei, S. Xu, T. Sun, S. Zeng, X. Guo, C. Song, Z. Liu, Tuning the product selectivity of SAPO-18 catalysts in MTO reaction via cavity modification, *Chinese, J. Catal.* 40 (2019) 477–485, [https://doi.org/10.1016/S1872-2067\(19\)63281-X](https://doi.org/10.1016/S1872-2067(19)63281-X).
- [49] A.T. Aguayo, A.G. Gayubo, R. Vivanco, M. Olazar, J. Bilbao, Role of acidity and microporous structure in alternative catalysts for the transformation of methanol into olefins, *Appl. Catal. A Gen.* 283 (2005) 197–207, <https://doi.org/10.1016/j.apcata.2005.01.006>.
- [50] D. Ali, Z. Li, M.M. Azim, H.L. Lein, K. Mathisen, Evaluating pore characteristics and acid site locations in hierarchical SAPO-11 by catalytic model reactions, *Microporous Mesoporous Mater.* 329 (2022), <https://doi.org/10.1016/J.MICROMESO.2021.111550>.
- [51] P. Pérez-Urriarte, M. Gamero, A. Ateka, M. Díaz, A.T. Aguayo, J. Bilbao, Effect of the acidity of HZSM-5 zeolite and the binder in the DME transformation to olefins, *Ind. Eng. Chem. Res.* 55 (2016) 1513–1521, <https://doi.org/10.1021/ACS.IECR.5B04477>.
- [52] T. Fu, H. Zhou, Z. Li, Controllable synthesis of ultra-tiny nano-ZSM-5 catalyst based on the control of crystal growth for methanol to hydrocarbon reaction, *Fuel Process. Technol.* 211 (2021), 106594, <https://doi.org/10.1016/J.FUPROC.2020.106594>.
- [53] Z. Han, F. Zhou, J. Zhao, Y. Liu, H. Ma, G. Wu, Synthesis of hierarchical GaZSM-5 zeolites by a post-treatment method and their catalytic conversion of methanol to olefins, *Microporous Mesoporous Mater.* 302 (2020), 110194, <https://doi.org/10.1016/J.MICROMESO.2020.110194>.
- [54] L. Tan, P. Zhang, Y. Cui, Y. Suzuki, H. Li, L. Guo, G. Yang, N. Tsubaki, Direct CO₂ hydrogenation to light olefins by suppressing CO by-product formation, *Fuel Process. Technol.* 196 (2019), 106174, <https://doi.org/10.1016/j.fuproc.2019.106174>.
- [55] G. Li, F. Jiao, X. Pan, N. Li, D. Miao, L. Li, X. Bao, Role of SAPO-18 acidity in direct syngas conversion to light olefins, *ACS Catal.* 10 (2020) 12370–12375, <https://doi.org/10.1021/ACSCATAL.0C03257>.
- [56] A.G. Gayubo, A.T. Aguayo, A. Alonso, J. Bilbao, Kinetic modeling of the methanol-to-olefins process on a silicoaluminophosphate (SAPO-18) catalyst by considering deactivation and the formation of individual olefins, *Ind. Eng. Chem. Res.* 46 (2007) 1981–1989, <https://doi.org/10.1021/ie061278o>.
- [57] A.T. Aguayo, D. Mier, A.G. Gayubo, M. Gamero, J. Bilbao, Kinetics of methanol transformation into hydrocarbons on a HZSM-5 zeolite catalyst at high temperature (400–550 °C), *Ind. Eng. Chem. Res.* 49 (2010) 12371–12378, <https://doi.org/10.1021/IE101047F>.
- [58] A.T. Aguayo, A.E.S. del Campo, A.G. Gayubo, A. Tarrío, J. Bilbao, Deactivation by coke of a catalyst based on a SAPO-34 in the transformation of methanol into olefins, *J. Chem. Technol. Biotechnol.* 74 (1999) 315–321, [https://doi.org/10.1002/\(SICI\)1097-4660\(199904\)74:4<315::AID-JCTB34>3.0.CO;2-G](https://doi.org/10.1002/(SICI)1097-4660(199904)74:4<315::AID-JCTB34>3.0.CO;2-G).
- [59] S.S. Arora, D.L.S. Nieskens, A. Malek, A. Bhan, Lifetime improvement in methanol-to-olefins catalysis over chabazite materials by high-pressure H₂ co-feeds, *Nat. Catal.* 1 (2018) 666–672, <https://doi.org/10.1038/S41929-018-0125-2>.
- [60] V. Paunović, V. Sushkevich, P. Rzepka, L. Artiglia, R. Hauert, S. Sik Lee, J.A. Vvan Bokhoven, Reactivation of catalysts for methanol-to-hydrocarbons conversion with hydrogen, *J. Catal.* 407 (2022) 54–64, <https://doi.org/10.1016/J.JCAT.2022.01.018>.
- [61] M. Guisnet, P. Magnoux, Organic chemistry of coke formation, *Appl. Catal. A Gen.* 212 (2001) 83–96, [https://doi.org/10.1016/S0926-860X\(00\)00845-0](https://doi.org/10.1016/S0926-860X(00)00845-0).
- [62] M. Ibáñez, P. Pérez-Urriarte, M. Sánchez-Contador, T. Cordero-Lanzac, A.T. Aguayo, J. Bilbao, P. Castaño, Nature and location of carbonaceous species in a composite HZSM-5 zeolite catalyst during the conversion of dimethyl ether into light olefins, *Catalysts.* 7 (2017) 254–266, <https://doi.org/10.3390/catal7090254>.
- [63] A.G. Gayubo, A.T. Aguayo, A.L. Morán, M. Olazar, J. Bilbao, Role of water in the kinetic modeling of catalyst deactivation in the MTG process, *AICHE J.* 48 (2002) 1561–1571, <https://doi.org/10.1002/aic.690480718>.
- [64] J. Valecillos, I. Hita, E. Sastre, A.T. Aguayo, P. Castaño, Implications of Co-feeding water on the growth mechanisms of retained species on a SAPO-18 catalyst during the methanol-to-olefins reaction, *ChemCatChem.* 13 (2021) 3140–3154, <https://doi.org/10.1002/CCTC.202100124>.
- [65] L. Yang, C. Wang, L. Zhang, W. Dai, Y. Chu, J. Xu, G. Wu, M. Gao, W. Liu, Z. Xu, P. Wang, N. Guan, M. Dyballa, M. Ye, F. Deng, W. Fan, L. Li, Stabilizing the framework of SAPO-34 zeolite toward long-term methanol-to-olefins conversion, *Nat. Commun.* 12 (2021) 4661, <https://doi.org/10.1038/S41467-021-24403-2>.
- [66] E. Epelde, M. Ibáñez, A.T. Aguayo, A.G. Gayubo, J. Bilbao, P. Castaño, Differences among the deactivation pathway of HZSM-5 zeolite and SAPO-34 in the transformation of ethylene or 1-butene to propylene, *Microporous Mesoporous Mater.* 195 (2014) 284–293, <https://doi.org/10.1016/j.micromeso.2014.04.040>.
- [67] T. Cordero-Lanzac, A. Ateka, P. Pérez-Urriarte, P. Castaño, A.T. Aguayo, J. Bilbao, Insight into the deactivation and regeneration of HZSM-5 zeolite catalysts in the conversion of dimethyl ether to olefins, *Ind. Eng. Chem. Res.* 57 (2018) 13689–13702, <https://doi.org/10.1021/acs.iecr.8b03308>.
- [68] M. Luo, B. Hu, G. Mao, B. Wang, Trace compounds confined in SAPO-34 and a probable evolution route of coke in the MTO process, *ACS Omega.* 7 (2022) 3277–3283, <https://doi.org/10.1021/ACSOMEGA.1C05336>.